ANTIOXIDANTS & REDOX SIGNALING
Volume 00, Number 00, 2015

DOI: 10.1089/ars.2014.6035

ORIGINAL RESEARCH COMMUNICATION

SOD3 Variant, R213G, Altered SOD3 Function, Leading to ROS-Mediated Inflammation and Damage in Multiple Organs of Premature Aging Mice

Myung-Ja Kwon,[1] Kyo-Young Lee,[2] Han-Woong Lee,[3] Jung-Ho Kim,[1] and Tae-Yoon Kim[1]

Abstract

Aims: Among the isoforms of superoxide dismutase, SOD3 is uniquely associated with the extracellular matrix (ECM) by virtue of its heparin-binding domain (HBD). Substitution of arginine by glycine at amino acid 213 (R213G) of its HBD was first identified in patients with heart failure, followed by many studies that focused on the role of this variant ($SOD3_{R213G}$) in ischemic heart disease and cardiovascular disease. However, the biological significance of this mutation in a physiological context is largely unknown. ***Results:*** As a first step, we generated $SOD3_{R213G}$ transgenic mice, in which the variant gene was driven by the β-actin promoter allowing expression in all tissues. Unexpectedly, we found that $SOD3_{R213G}$ transgenic mice exhibited premature aging, including hair graying, abnormal gait, and a shortened life span. Specifically, the aged mice showed systemic inflammation and organ degeneration. In addition, aged $SOD3_{R213G}$ mice are susceptible to neutrophil-mediated inflammation. Among other functions, the neutrophils of $SOD3_{R213G}$ mice produce high amounts of reactive oxygen species, which would normally be controlled by SOD3 in ECM. ***Innovation:*** These findings showed for the first time that arginine 213 in the HBD of SOD3 is critical for maintaining proper organ function through moderating the normal innate immune response, which would otherwise lead to chronic inflammation and degenerative diseases in aged mice. ***Conclusion:*** Therefore, patients with this variant may be treated with SOD3 as a therapeutic strategy to prevent or cure these diseases.

Introduction

SUPEROXIDE DISMUTASE 3 (SOD3) is an antioxidant enzyme that scavenges superoxide and other reactive oxygen species (ROS) produced in cells and tissues preventing cell death and protecting normal tissue during inflammation (29). Unlike other SODs, SOD3 is a glycoprotein with a heparin-binding domain (HBD). SOD3 is predominantly expressed in the extracellular matrix (ECM) of tissues and the glycocalyx of cell surfaces, where it is anchored to heparan sulfate proteoglycan (27, 28, 38). Since SOD3 is highly expressed in normal lung tissue, blood vessels, airways, kidneys, the uterus, and the heart (17, 41), the role of SOD3 in protection against oxidative stress in these organs is well established (7, 44). In addition, we have demonstrated that SOD3 acts to modulate the innate and adaptive immune re-

Innovation

We report that aged $SOD3_{R213G}$ Tg mice exhibit hair graying, abnormal gait, and shortened life span. Specifically, the aged mice had systemic inflammation with degeneration of organs. Aged $SOD3_{R213G}$ mice are susceptible to neutrophil-mediated inflammation. These innate immune cells possess strong chemotactic and apoptotic and proinflammatory characters, producing higher levels of reactive oxygen species, in response to bacterial fragments. These features may contribute to the expression of the phenotype. Thus, these unexpected findings demonstrate that arginine 213 is required for proper SOD3 function and SOD3 has a role in regulating chronic inflammation and degenerative diseases, including organismal aging.

[1]Department of Dermatology, Catholic Research Institute of Medical Science, College of Medicine, The Catholic University of Korea, Seoul, Republic of Korea.
[2]Department of Hospital Pathology, College of Medicine, The Catholic University of Korea, Seoul, Republic of Korea.
[3]Department of Biochemistry, College of Life Science and Biotechnology, Yonsei University, Seoul, Republic of Korea.

sponses, meliorating the progression of skin diseases and airway inflammation (22, 23). Considering that the ECM is essential for tissue homeostasis and that any changes in the ECM microenvironment can be detrimental to cell function, SOD3 may play a critical role in protection against external environmental factors such as pathogens.

The SOD3 variant, R213G, is a common human gene variant, which involves the substitution of arginine by glycine at amino acid 213 (R213G) in the HBD (19, 30). This variant is associated with increased risk of ischemic heart diseases (19), vascular impairment (11), and lung inflammation (2), and many molecular aspects of the mutant R213G of SOD3 in these diseases have been studied (11, 25, 26, 34). However, the biological significance of this variant and relevance in a physiological setting are largely unknown. In addition, the impacts of this mutation on premature aging, systemic inflammation, and cellular degeneration have not been investigated.

The skin, lung, and intestine are the first defensive barriers against pathogens. Failure of these defenses leads to infection, causing systemic inflammation. In addition, neutrophils are the first line of defense against infections caused by bacteria, fungi, and parasites, which rapidly initiate innate immune responses to clear pathogens *via* chemotaxis or phagocytosis, producing ROS (10). On the other hand, these cells exhibit plasticity upon stimulation (32) and secrete extracellular remodeling substances, including elastase, cathepsin G, and proinflammatory cytokines, which cause tissue damage (4, 33).

In addition, as a natural aging-associated feature, hair graying occurs by loss of pigment in the hair shaft caused by impairment of melanogenesis, antioxidant mechanisms, or antiapoptotic signals (42). Specifically, melanocytes in graying hair bulbs are frequently highly vacuolated due to oxidative stress (3). Furthermore, ROS-mediated damage of melanocytes leads to hair graying (14). Although SOD3 has antioxidative and anti-inflammatory effects, the impact of variant R213G of SOD3 on these events has not yet been reported.

In this study, we reported for the first time that $SOD3_{R213G}$ Tg mice exhibit premature aging, including hair graying and abnormal gait, and shortened life span. Specifically, the aged mice had systemic inflammation and degeneration of aortic myocytes and the femoral growth plate. Tissue-infiltrating neutrophils were significantly increased in the aged $SOD3_{R213G}$ mice. Interestingly, the distinctive phenotype of $SOD3_{R213G}$ mice was not simply due to the alteration of SOD enzyme activity. Instead, we observed that $SOD3_{R213G}$ mice released SOD3 into the blood. These results suggest that arginine 213 of SOD3 is critical for the proper function of SOD3 in the prevention of inflammatory and degenerative diseases that occur during aging. Given the important role of the arginine 213 mutation in SOD3, patients with this variant may be treated with SOD3 as a therapeutic strategy to prevent or cure these diseases.

Results

Generation of $SOD3_{R213G}$ transgenic mice

To study the physiological relevance of $SOD3_{R213G}$, we generated transgenic (Tg) mice with the human SOD3 variant, R213G, driven by the β-actin promoter to ensure tissue-wide expression. The Tg mice were generated using a high-level constitutively expressed SOD3 variant, R213G, substituting arginine by glycine at amino acid 213 in the HBD, driven by the chicken β-actin promoter of pCAGGS vector. The expression cassette contained the CMV-IE enhancer, chicken β-actin promoter, and human $SOD3_{R213G}$ cDNA, followed by a rabbit β-globin polyadenylation site (Fig. 1A). The transgene was purified and microinjected into pronuclei of fertilized eggs from C57BL/6J mice. For the experimental control, SOD3 or SOD3 lacking HBD Tg mice were generated by inserting either human SOD3 or SOD3 lacking HBD into the same plasmid backbone of $SOD3_{R213G}$ Tg mice. To confirm the Tg mice, the genotype was determined by PCR amplification using genomic DNA of tail biopsies with a primer recognizing part of hSOD3 and the rabbit β-globin poly A tail, 5′-gacggcagcctctggaggta; 3′-catggcagccagcatatggc. The top band (Fig. 1B, 540 bp) was cut out, and sequencing analysis was performed to confirm the mice (Fig. 1C, Gene Biotech, Seoul, Korea).

As shown in Figure 1D, two founders, #44 and #47, which have less than ten copy numbers of the transgene, were selected. Through a restriction enzyme PCR-based technique (9), the insertion site of the transgene was identified and it revealed that the transgene of founder #44 was integrated at the noncoding region of chromosome 10 and the gene of founder #47 was integrated at chromosome 7 (AL 772165.15) and uncharacterized locus (XR 404620) (Fig. 1E), respectively. Thus, although the gene insertion was different between the two founders, the mice showed the same phenotype, suggesting that the distinctive phenotype of the mice is not due to gene insertion. Furthermore, the transgene was significantly overexpressed in the organs of $SOD3_{R213G}$ Tg mice, while expression of endogenous SOD3 was lower (Fig. 1F).

$SOD3_{R213G}$ Tg mice exhibit shortened life span and hair graying

Surprisingly, $SOD3_{R213G}$ Tg mice exhibited a shortened life span (Fig. 1H) with their hair turning gray upon aging (Fig. 1G). The mean life span of the Tg mice was 11 months. In addition, 17-week-old Tg mice had higher numbers of white blood cells and elevated aspartate aminotransferase, alanine aminotransferase, creatine phosphokinase, glucose, and low-density lipoprotein levels than those of same-aged wt mice (Table 1), implying that the aged mutant mice had an inflammatory pathology.

Arginine 213 of SOD3 is required for proper melanocyte proliferation and melanogenesis

Histopathological examinations and FACS analysis revealed that aged $SOD3_{R213G}$ Tg mice had reduced levels of melanin in the hair follicles, including the hair bulb and shaft (Fig. 2A), as well as fewer melanocytes than wt mice (Fig. 2B), responsible for hair graying. To examine the mechanism, we used Melan A cells (5) that were transiently transfected with plasmids encoding human SOD3, SOD3 lacking HBD, or SOD_{R213G} mutant. When cell proliferation was assessed by stimulation with PMA, cells overexpressing SOD3 exhibited enhanced cell proliferation and cells expressing SOD3 lacking HBD maintained proliferation at the control levels (Fig. 2C, D), while cells expressing the mutant drastically inhibited proliferation. A possible explanation was that

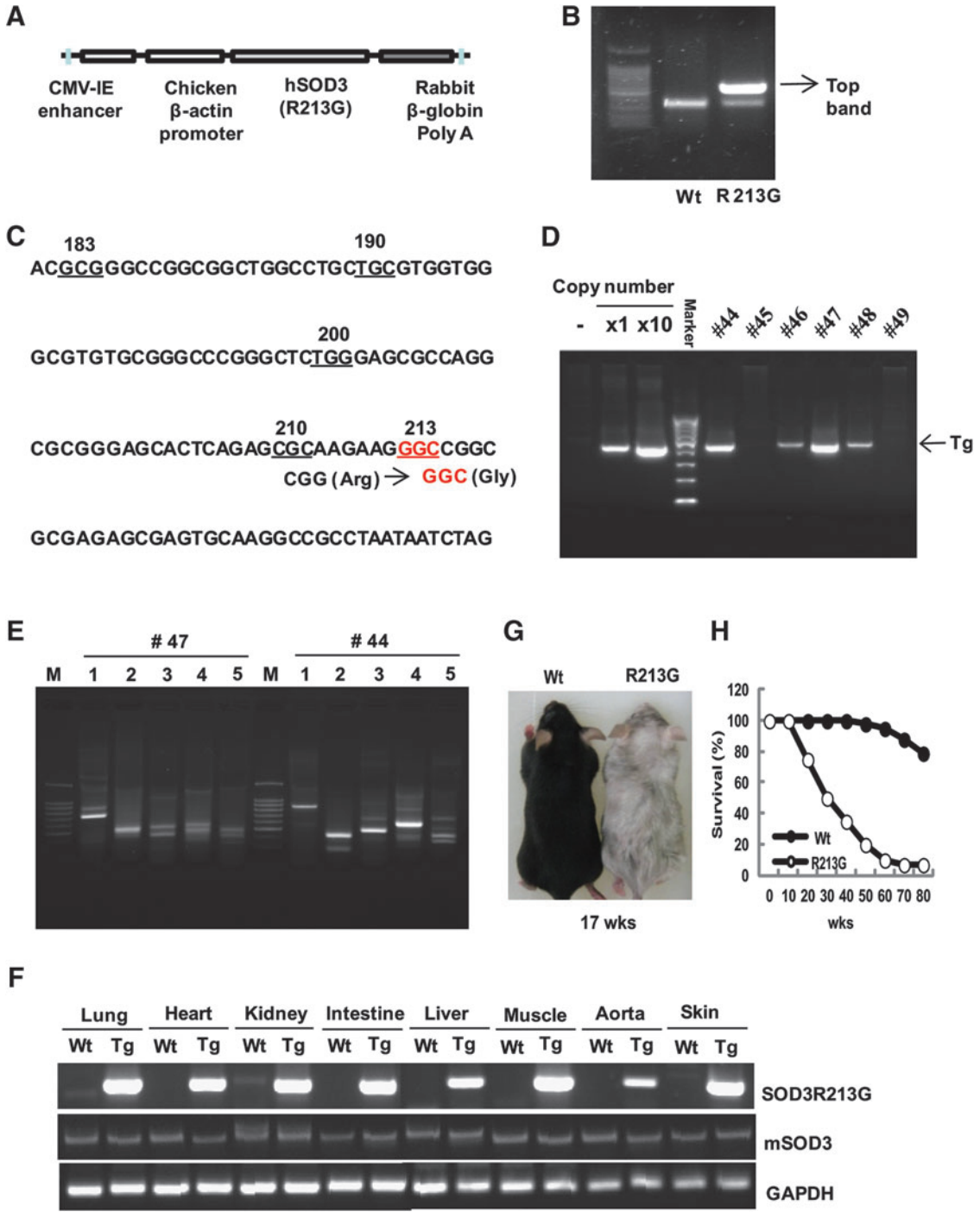

FIG. 1. Generation of SOD3 $_{R213G}$ mutant Tg and their phenotypes. **(A)** The structure of the $SOD3_{R213G}$ mutant Tg construct. The R213G construct was cloned into the pCAGGS vector. Tg mice were generated as described in the Materials and Methods section. **(B, C)** Confirmation of $SOD3_{R213G}$ Tg mice. The genotype was determined by PCR amplification using genomic DNA of tail biopsies **(B)**, and the sequence was confirmed as described in the Materials and Methods section **(C)**. **(D)** Copy number of $SOD3_{R213G}$ mutant Tg mice. **(E)** Identification of the insertion site of the transgene of two founders. The insertion site of the transgene was identified by a restriction enzyme-based PCR technique as described in the Materials and Methods section. Indicated number in the figure represents the restriction enzyme; 1:Hind III, 2:Pvu I, 3:SacI, 4: BgI II, 4:Pst 1. **(F)** Expression of exogenous and endogenous SOD3 in $SOD3_{R213G}$ mice. **(G)** Seventeen-week-old $SOD3_{R213G}$ mice showed hair graying. **(H)** Kaplan–Meier survival curve. *Closed circles* are Wt mice; *open circles* are $SOD3_{R213G}$ mice. Each of the forty wt or $SOD3_{R213G}$ mice was monitored. To see this illustration in color, the reader is referred to the web version of this article at www.liebertpub.com/ars

Table 1. Serum Profiles of 17-Week-Old Wild-Type and $SOD3_{R213G}$ Mutant Mice

	WBC(103/μl)	*AST(IU/L)*	*ALT(IU/L)*	*CPK(IU/L)*	*GLU(mg/dl)*	*TG(mg/dl)*	*LDL(mg/dl)*
WT	1.7 ± 0.2	49.2 ± 5.6	24.6 ± 5.1	59.5 ± 19.5	205.1 ± 15.1	95.06 ± 13.4	15.25 ± 1.7
TG	2.9 ± 1.0	68.5 ± 7.0*	36.7 ± 4.8	108 ± 16.7*	277.4 ± 10.4*	73.75 ± 7.3	26.5 ± 3.8

Blood was obtained from the periorbital sinus of the mice. Blood count and biochemical analysis of serum enzymes and lipids were performed using VetAce (Alfa Wassermann system). The sample included six males of Wt and $SOD3_{R213G}$ mutant mice. Statistical significance (*) was determined by Student's *t*-test at $p < 0.01$.

CPK, creatine phosphokinase; Glu, glucose; LDL, low-density lipoprotein.

$SOD3_{R213G}$-expressing cells exhibited increased apoptosis (Fig. 2E). In agreement, the corresponding proliferation genes, *c-Myc* and *cyclin D1*, were downregulated, but *Bax* was upregulated in $SOD3_{R213G}$-expressing cells (Fig. 2G–I). However, aging marker, telomerase reverse transcriptase (TERT), expression was not significantly changed by $SOD3_{R213G}$ (Fig. 2F).

To explore the defect in melanogenesis, we determined the levels of the microphthalmia transcription factor (*MITF*) that controls melanocyte differentiation, including expression of tyrosinase *(Tyr)* and dopachrome tautomerase (*Dct)* (6, 45). While SOD3-expressing cells upregulated *MITF* expression, cells expressing SOD3 lacking HBD maintained the basal level of *MITF* expression (Fig. 2J), and $SOD3_{R213G}$-expressing cells inhibited *MITF* expression (Fig. 2J). In agreement with this finding, consistent expression patterns were observed for its corresponding genes, *Tyr* and *Dct* (Fig. 2K, L), suggesting that SOD3 controls melanogenesis and arginine 213 is essential for the function of SOD3.

$SOD3_{R213G}$ mice develop chronic skin inflammation and cellular degeneration upon aging

Skin is the first defensive barrier against pathogens, and failure of defense leads to infection. Thus, we speculated that pathogenic conditions of aged mutant mice might be due to a failure of this defense. To test this, we first investigated the skin of the aged mutant mice maintained in a semispecific pathogen-free facility. Indeed, aged Tg mice had skin inflammation with increased numbers of infiltrated inflammatory cells (Fig. 3A, first lower panel) and focally thickened epidermis (Fig. 3A, second lower panel) accompanied by inflammation and fibrosis in the dermis (Fig. 3A, second lower panel), muscle atrophy (Fig. 3A, third lower panel), and increased numbers of apoptotic cells in the epidermis (Fig. 3B, left panel) and hair follicles (Fig. 3B, right panel). However, these phenotypes were not observed in wt mice (Fig. 3A, upper panels).

For detail investigation, transmission electron microscopy analysis was applied, which showed that the skin of the mutant mice had empty spaces created by dead cells in the dermis (Fig. 3C, first panel) and apoptotic cells in both the epidermis and dermis (Fig. 3C, second to fifth panels). In addition, Masson's trichrome staining showed that the skin of the aged Tg mice had chronic inflammation with edema in the deep dermis (Fig. 3D, third panel) and increased collagen deposition in the deep subcutaneous tissue and intermuscular stroma (Fig. 3D, fourth panel). However, these phenotypes were not observed in wt mice (Fig. 3D, first and second panels). The corresponding proinflammatory gene, TNFα (Fig. 3E), dermal matrix remodeling molecular matrix metalloproteinase-1 (MMP-1) (Fig. 3F), monocyte chemoattractant, monocyte chemotactic protein 1 (MCP-1) (Fig. 3G), and neutrophil chemoattractant, MIp1α (Fig. 3H), were all upregulated. In addition, aging marker, TERT, was upregulated (Fig. 3I). Taken together, $SOD3_{R213G}$ mice developed chronic skin inflammation and cellular degeneration upon aging. Therefore, these results suggest that SOD3 can protect against skin infection and that arginine 213 of SOD3 is essential for the function of SOD3 in the skin.

Infiltrating neutrophils are significantly increased in $SOD3_{R213G}$ Tg mice upon aging, along with upregulation of proinflammatory cytokines

To further investigate the cause of skin and organ inflammation in $SOD3_{R213G}$ mice, immunofluorescence imaging analysis was applied. As shown in Figure 4A, infiltrating neutrophils and macrophages were highly increased in the skin of aged mutant mice compared with Wt (Fig. 4A, second and third panels). Since failure of the first line of defense may lead to systemic inflammation, we also observed increased numbers of neutrophils, macrophages, and lymphocytes in the blood (Fig. 4B), bronchoalveolar lavage fluid (BALF) in the lung (Fig. 4C), and the spleen (Fig. 4D) of the aged Tg mice. Correspondingly, increased levels of proinflammatory cytokines, IL-6 (Fig. 4E, upper panel) and TNFα (Fig. 4E, lower panel), were observed in $SOD3_{R213G}$ mice.

$SOD3_{R213G}$ promotes the levels of circulating and infiltrating neutrophils in organs of the aged mice, while SOD enzyme activity is unaffected and SOD3 level is increased in blood

We, next, compared the phenotype of $SOD3_{R213G}$ mice with that of age-matched SOD3 Tg, SOD3 lacking HBD, and SOD3 Ko mice. SOD3 Tg mice had fewer inflammatory cells in the blood (Fig. 5A), BALF (Fig. 5B), and spleen (Fig. 5C and Supplementary Fig. S1A; Supplementary Data are available online at www.liebertpub.com/ars). However, increased levels of circulating and infiltrated cells, specifically neutrophils, were dominantly observed in aged $SOD3_{R213G}$ mice (Fig. 5A–C and Supplementary Fig. S1A). Consistently, higher levels of proinflammatory cytokines, IL-6, IL-4, IL-13, and TNFα, were observed in these mutant mice (Supplementary Fig. S1B). Although SOD3 Ko mice have similar patterns, the levels of neutrophils and proinflammatory cytokines were less than those of $SOD3_{R213G}$ mice (Fig. 5A–C and Supplementary Fig. S1). In addition, mice expressing SOD3 lacking HBD had a similar phenotype to that of SOD3 Tg mice (Fig. 5A–C and Supplementary Fig. S1A, B). Interestingly, the content of neutrophils in the bone marrow of $SOD3_{R213G}$ mice was not significantly different, compared

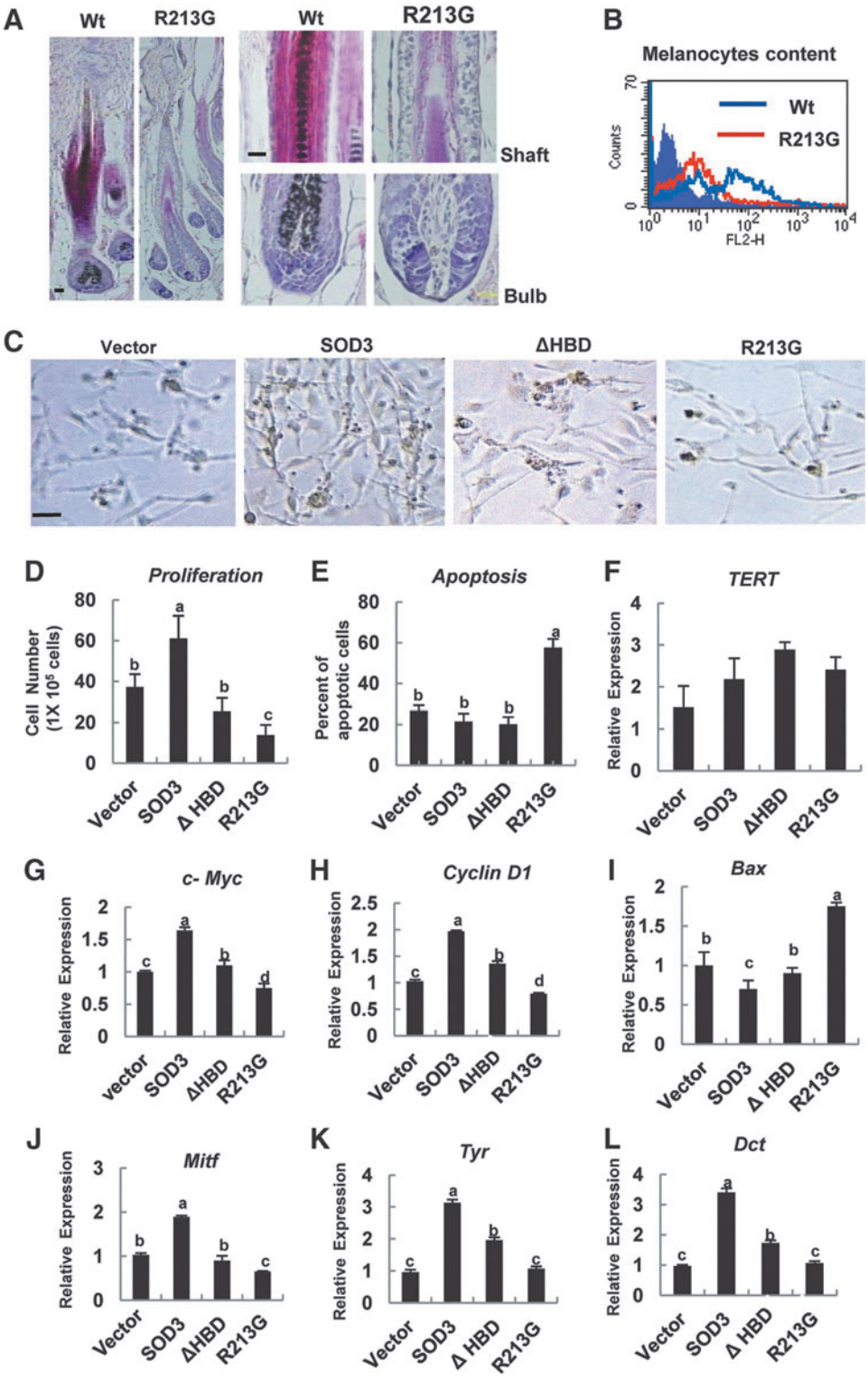

FIG. 2. $SOD3_{R213G}$ mutant mice exhibit hair graying. (A) Aged $SOD3_{R213G}$ mice lack melanin pigment in hair follicles. Dorsal skin sections of 17-week-old $SOD3_{R213G}$ mice were isolated, and H&E staining was followed. Scale bar, 200 μm (*left panel*) and 20 μm (*right panel*) **(B)** Melanocyte content in the skin. Single cells were separated from the skin as described in the Materials and Methods section. The cells were stained with PE-conjugated anti-Melan A antibody, and FACS analysis was followed. **(C–F)** Proliferation **(C, D)**, apoptosis **(E)**, and TERT **(F)** expression of melanocytes. Scale bar, 200 μm. **(G–J)** Expression of *c-Myc* **(G)**, *Cyclin D1* **(H)**, and *Bax* **(I)**. **(J–L)** The expression of melanogenesis-related genes: Microphthalmia-associated transcription factor *(MITF)* **(J)**, *tyrosinase (Tyr)* **(K)**, and *dopachrome tautomerase (Dct)* **(L)**. Melan A cells were transiently transfected as described in the Materials and Methods section. Cell proliferation and apoptosis and expression of the indicated genes were assessed as described in the Materials and Methods section. The *in vitro* data represent the mean ± SD of at least three independent experiments. Statistical analysis was performed by ANOVA at $p < 0.01$, and Scheffe's *post hoc* test was followed; grouping a, b, c, and d. To see this illustration in color, the reader is referred to the web version of this article at www.liebertpub.com/ars

with wt, SOD3 Tg, SOD3 lacking HBD, and SOD3 Ko mice (Fig. 5D), implying that $SOD3_{R213G}$ may promote proliferation or increase trafficking of neutrophils. Surprisingly, $SOD3_{R213G}$ did not affect SOD enzyme activity (Fig. 5E). Instead, we observed that a higher amount of SOD3 was released into the blood of $SOD3_{R213G}$ mice (Fig. 5F). Therefore, these results imply that the distinctive phenotype of $SOD3_{R213G}$ mice may not simply be due to alteration of SOD enzyme activity, but it may be due to releasing of SOD3 from tissue into the blood.

The SOD3 variant, R213G, leads to aberrant neutrophil function in mice

We next investigated the function of neutrophils of $SOD3_{R213G}$ mice by treatment with the bacterial fragment,

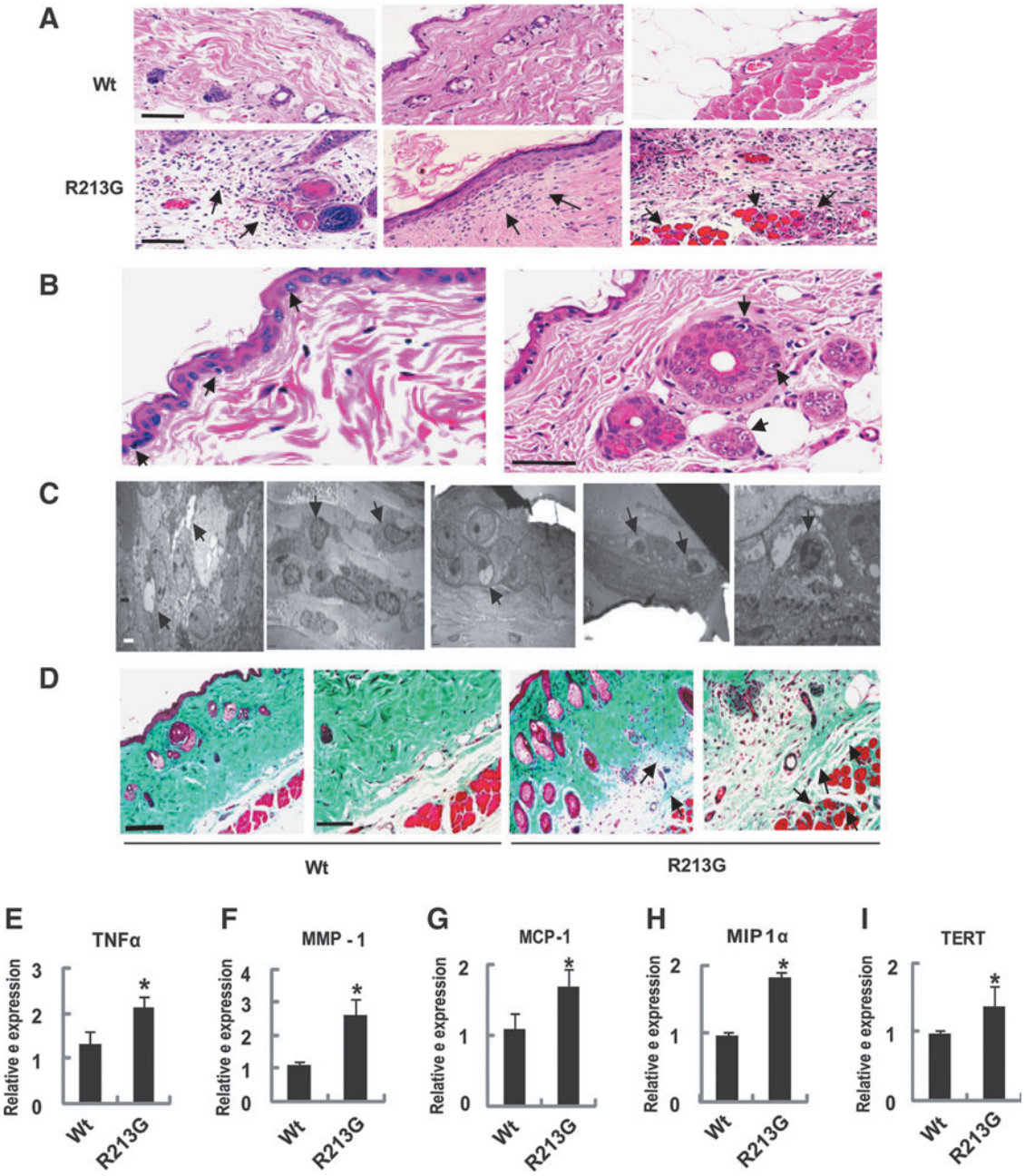

FIG. 3. $SOD3_{R213G}$ mice develop chronic skin inflammation and cellular degeneration upon aging. **(A, B)** Severe skin inflammation of aged $SOD3_{R213G}$ mice. The dorsal skin of 17-week-old $SOD3_{R213G}$ or Wt mice was isolated, and H&E staining was followed. Increased numbers of inflammatory cells **(A**, *first lower panel*), fibrosis **(A**, *second lower panel*), focally thickened epidermis **(A**, *second lower panel*), and muscle atrophy **(A**, *third lower panel*) were observed. Scale bar, 100 μm. Degenerative cells, including nuclear condensed cells in the epidermis **(B**, *left panel*) and hair follicles **(B**, *right panel*) of aged $SOD3_{R213G}$ mice. Scale Bar, 50 μm. **(C)** Degenerative cells in the skin of aged $SOD3_{R213G}$ mice. Dead cell-created spaces **(C**, *first panel*) and necrotic cells **(C**, *second panel*) in the dermis, vacuolated cells **(C**, *third panel*) in the epidermis, and nucleus condensed cells **(C**, *fourth and fifth panels*) in the epidermis were observed by TEM as described in the Materials and Methods section. Scale bar, 2 μm. **(D)** Chronic skin inflammation of aged $SOD3_{R213G}$ mice. Chronic inflammation with edema in the deep dermis **(D**, *third panel*) and increased collagen deposition in the deep subcutaneous tissue and intermuscular stroma **(D**, *third and fourth panels*) of aged $SOD3_{R213G}$ mice were observed by Masson's trichrome staining. Scale bar, 100 μm (*left panels* of each Wt and $SOD3_{R213G}$) and 50 μm (*right panels* of each Wt and $SOD3_{R213G}$). **(E–I)** Expression of inflammatory and aging-related genes: Proinflammatory cytokines, TNFα **(E)**; dermal matrix remodeling factor, MMP1 **(F)**; inflammatory chemokine, MCP-1 **(G)**; chemoattractant toward neutrophils, MIP1a **(H)**; and aging-related gene, TERT **(I)**. The expression of indicated genes was performed by quantitative PCR as described in the Materials and Methods section. Statistical analysis was performed by *t*-test (*$p < 0.001$ *vs.* wt control). *Arrows* indicate infiltrated cell and fibrosis **(A)**, apoptotic cell **(B)**, condensed cell **(C)**, and collagen accumulation **(D)**. To see this illustration in color, the reader is referred to the web version of this article at www.liebertpub.com/ars

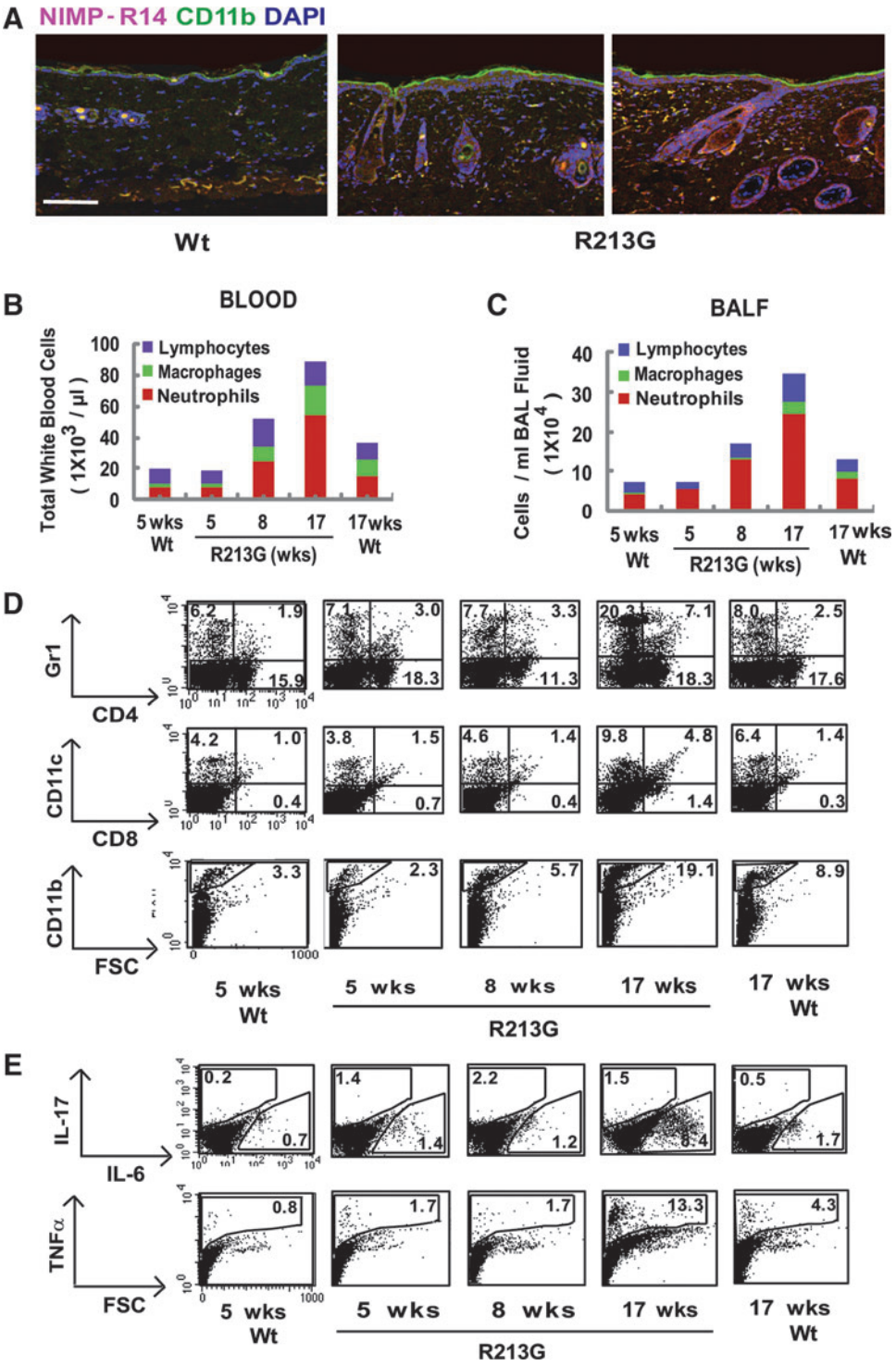

FIG. 4. Infiltration of innate immune cells and expression of proinflammatory cytokines in aged $SOD3_{R213G}$ mice. **(A)** Infiltrating neutrophils and macrophages are in the skin of aged $SOD3_{R213G}$ mice. The dorsal skin of 17-week-old $SOD3_{R213G}$ mice was isolated, and immunofluorescence staining and confocal analysis were performed as described in the Materials and Methods section. NIMP-R14: neutrophil; CD11b: macrophage, Scale bar, 100 μM. **(B, C)** Neutrophils are dominantly increased in blood and bronchoalveolar lavage fluid (BALF) of $SOD3_{R213G}$ mice upon aging. Neutrophil, macrophage, and lymphocyte contents in blood **(B)** and BALF **(C)** in the lung of $SOD3_{R213G}$ mice. Blood **(B)** and BALF **(C)** were obtained from mice and deep quick staining and differential cell counting based on cell morphology were performed. **(D)** Changes in the population of immune cells in the spleen of $SOD3_{R213G}$ mice upon aging. Population of $Gr1^+$ and $CD4^+$ (*upper panel*), $CD11c^+$ and $CD8^+$ (*middle panel*), and $CD11b^+$ (*lower panel*) in the spleen of $SOD3_{R213G}$ mice upon aging. **(E)** Changes in the levels of proinflammatory cytokines, IL-17 and IL-6 (*upper panel*) and TNFα (*lower panel*). Each of the 5- or 17-week-old wt mice was used as a control. To see this illustration in color, the reader is referred to the web version of this article at www.liebertpub.com/ars

formyl-methionyl-leucyl-phenylalanine (fMLP) (40). Upon stimulation with fMLP, the neutrophils underwent increased apoptosis (Fig. 6A), chemotactic ability (Fig. 6B), and elastase expression (Fig. 6C). These levels were greater than those of wt, SOD3 Tg, SOD3 lacking HBD, and SOD3 Ko mice. In addition, $SOD3_{R213G}$ neutrophils upregulated the expression of proinflammatory molecules, TNFα (Fig. 6D), IL-6 (Fig. 6E), and cathepsin G (Fig. 6F). A similar pattern was observed in SOD3 Ko mice (Fig. 6D–F), but the level was lower than those of aged $SOD3_{R213G}$ mice. However, the levels of wt, SOD3 Tg, and SOD3 lacking HBD Tg mice were comparably low (Fig. 6D–F). Consistently, most neutrophils of $SOD3_{R213G}$ mice possess a proinflammatory phenotype (21), $Gr1^{high}$ $CD11b^{high}CXCR4^{low}$ (Fig. 6G).

When neutrophils isolated from the bone marrow of $SOD3_{R213G}$ Tg mice were treated with G-CSF, the cells appeared large and blast-like (Fig. 6H). A similar phenotype was observed in neutrophils of SOD3 Ko mice (Fig. 6H),

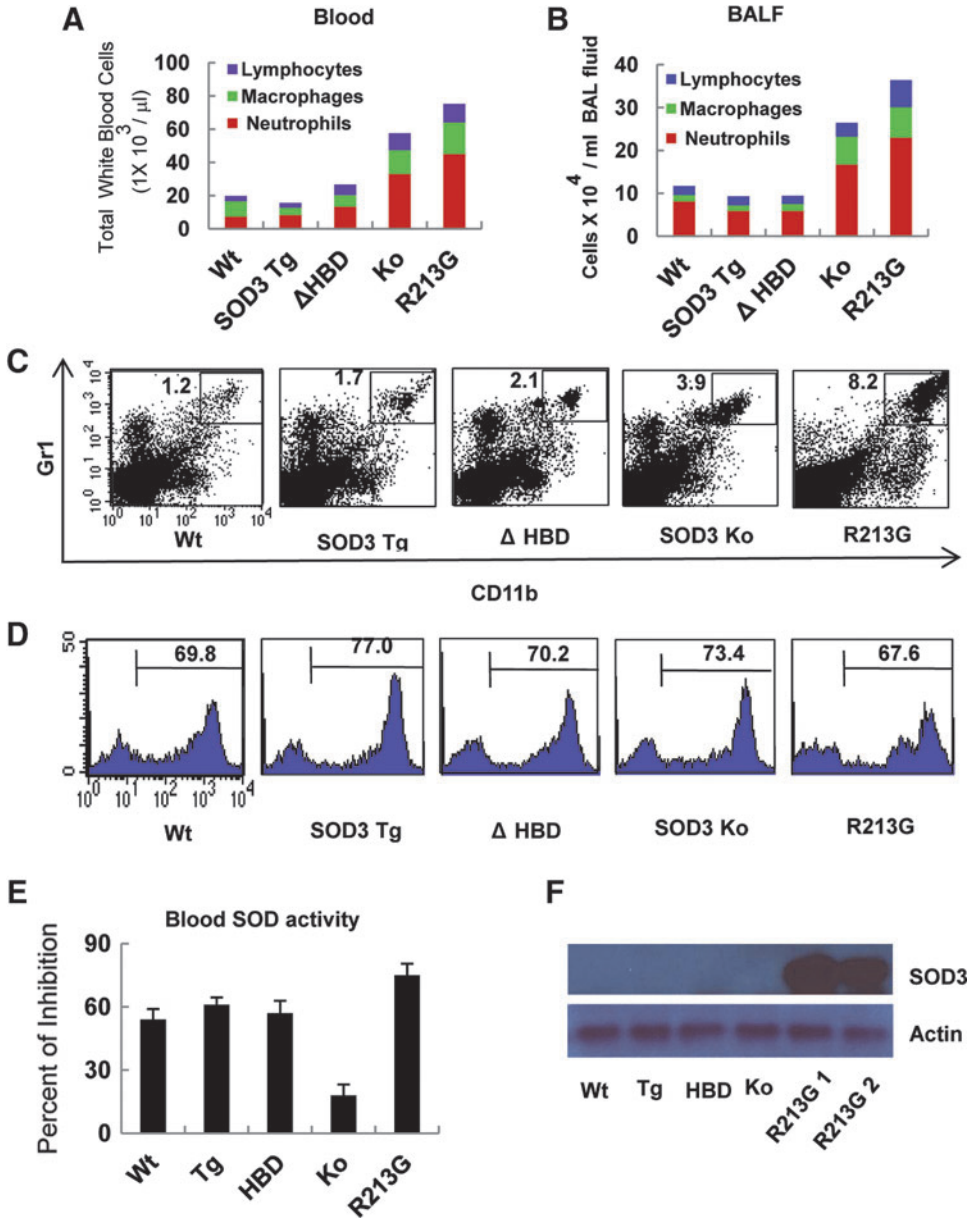

FIG. 5. $SOD3_{R213G}$ promotes the levels of circulating and infiltrating neutrophils in organs of the aged mice, while SOD enzyme activity is unaffected and SOD3 level is increased in blood. (A, B) Comparison of cell profiles in blood **(A)** and BALF **(B)**. **(C)** The population of $Gr1^+CD11b^+$ neutrophils in the spleen. **(D)** Neutrophil content in the bone marrow. Indicated cell profiles of either spleen or bone marrow of 17-week-old $SOD3_{R213G}$ mice, including corresponding aged wt, SOD3 Tg, SOD3 lacking HBD, and SOD3 Ko mice, were assessed by FACS analysis as described in the Materials and Methods section. ΔHBD: SOD3 lacking HBD mice, Ko: SOD3 Ko mice, R213G: $SOD3_{R213G}$ mice. **(E, F)** SOD activity, and released SOD3 into the blood. SOD3 activity **(E)** and SOD 3 level **(F)** in the blood. R213G1 and R213G2 represent two different $SOD3_{R213G}$ mice. SOD activity in the blood was measured as described in the Materials and Methods section. SOD3 in the blood was detected by SDS-PAGE as mentioned in the Materials and Methods section. To see this illustration in color, the reader is referred to the web version of this article at www.liebertpub.com/ars

suggesting that SOD3 is required for proper neutrophil differentiation and proliferation. In addition, these blast-like cells from $SOD3_{R213G}$ mice produced higher levels of ROS upon stimulation with fMLP compared with neutrophils from wt, SOD3 Tg, SOD3 lacking HBD, and SOD3 Ko mice (Fig. 6I). Consistently, we observed that NADPH oxidase is sustained in $SOD3_{R213G}$ mice (Supplementary Fig S2). Furthermore, mouse embryo fibroblast of $SOD3_{R213G}$ mice showed increased ROS production (Supplementary Fig S2). Therefore, these results suggest that SOD3 is required for proper neutrophil development and homeostasis, which in turn, may mediate a normal innate immune response.

Aged $SOD3_{R213G}$ mice develop systemic inflammation and cellular degeneration

We further investigated other age-related changes in $SOD3_{R213G}$ mice. Through histopathological examination, we found that seven of the ten mice exhibited chronic inflammation in the skin, lung, gastric intestine, kidney, liver, muscle, and heart. Specifically, as shown in Figure 7A and B, inflammation in the peribronchovascular area and blood vessels of the lung (A, first panel) and destruction of tubular structures due to focal infiltration of chronic inflammatory cells in the cortex of the kidney (A, second panel), the interstitium of the muscle (A, third panel) and heart (B, first panel), and in the portal area of the liver (B, second panel) were observed in aged $SOD3_{R213G}$ mice. In addition, infiltration and aggregation of lymphocytes in the lamina propria of the intestine (B, third panel) were observed in these aged Tg mice. Furthermore, these phenotypes were more severe than those seen in SOD3 Ko mice (data not shown), which may lead to a shortened life span of the mice.

Surprisingly, severe degeneration of the aortic myocytes, smooth muscle cells in the media layers, was observed in aged $SOD3_{R213G}$ mice (Fig. 7C, first row, second panel), which may lead to failure of the function of the arterial wall, causing

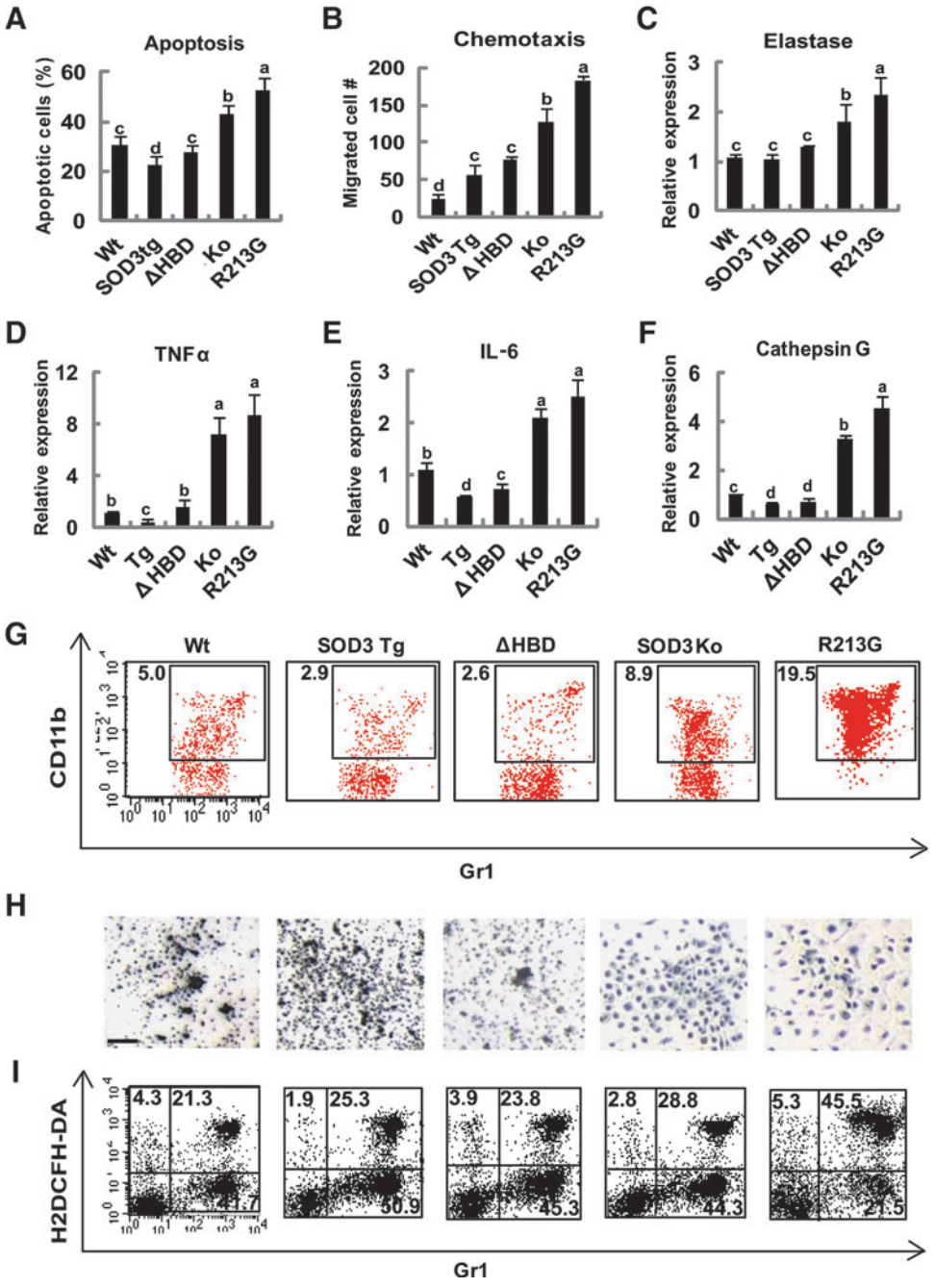

FIG. 6. Aberrant characteristics of neutrophils in aged $SOD3_{R213G}$ mice. (**A–C**) The characteristics of neutrophils in aged $SOD3_{R213G}$ mice. Potent apoptotic (**A**) and chemotatic (**B**) character and upregulation of elastase expression (**C**). Bone marrow-isolated neutrophils were treated with 100 n*M* fMLP for 8 h, and apoptosis (**A**) was assessed as described in the Materials and Methods section. Chemotaxis (**B**) was measured as described in the Materials and Methods section. (**D–F**) The expression of proinflammatory molecules: Neutrophils expressed proinflammatory molecules, TNFα (**D**), IL-6 (**E**), and cathepsin G (**F**). The gene expression of neutrophil elastase (**C**), TNFα (**D**), IL-6 (**E**), and cathepsin G (**F**) was assessed by treatment with 100 n*M* fMLP for 8 h and performed by qRT-PCR. (**G**) Neutrophils of $SOD3_{R213G}$ mice possess proinflammatory character. The $Gr1^{high}$ $CD11b^{high}$ $CXCR4^{low}$ cell population (**G**) was measured by FACS analysis, gating $Gr1^{high}$ $CXCR4^{low}$ and accessing the $CD11b^{high}$ population from BM cells. (**H**) Blast-like neutrophils in aged $SOD3_{R213G}$ mice. Neutrophils (**H**) of aged $SOD3_{R213G}$ mice are compared with those of wt, SOD3 Tg, SOD3 lacking HBD, and SOD3 Ko mice. Bone marrow-derived neutrophils were treated with G-CSF as described in the Materials and Methods section. The morphological image was taken by light microscopy. Scale bar, 200 μm. (**I**) Neutrophils of aged $SOD3_{R213G}$ mice promote reactive oxygen species (ROS) production. ROS generation (**I**) was assessed by treatment with fMLP (100 n*M*, 1 h) in BM cells and performed by staining with H_2DCFH-DA, 2′,7′-dichlorofluorescein diacetate (5 μ*M*) and APC-conjugated Gr1 antibody, and FACS analysis was followed. For the *in vitro* bar graph, results are the mean ± SD of at least three independent experiments. Statistical analysis was performed by ANOVA at $p < 0.01$, and Scheffe's *post hoc* test was followed; grouping a, b, c, and d. To see this illustration in color, the reader is referred to the web version of this article at www.liebertpub.com/ars

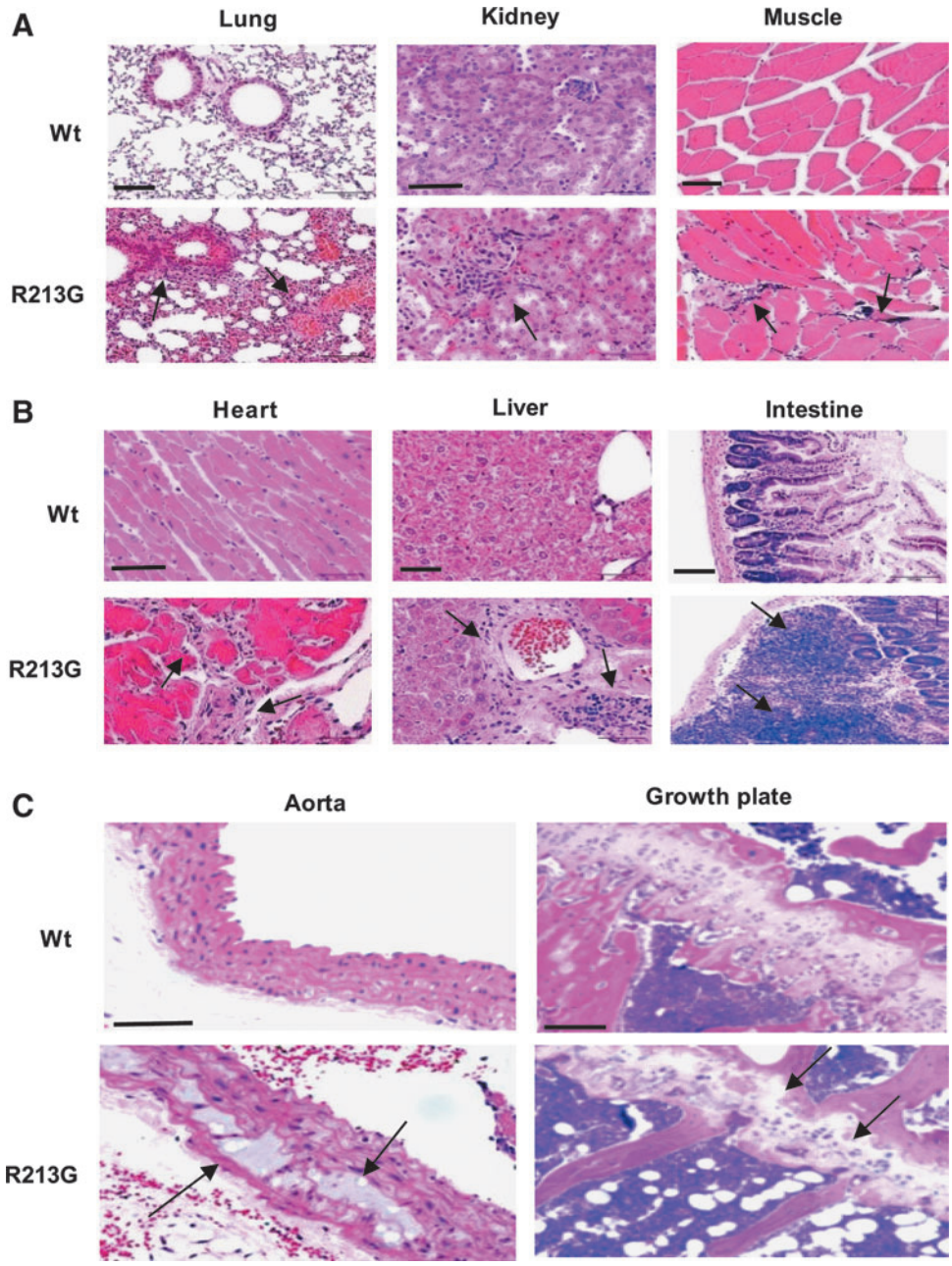

FIG. 7. Systemic inflammation and cellular degeneration occur in aged $SOD3_{R213G}$ mice. (A, B) Systemic inflammation in aged $SOD3_{R213G}$ mice. **(C)** Degeneration of myocytes in the aorta and growth plate in the femur of aged $SOD3_{R213G}$ mice. Histological analysis of the aged $SOD3_{R213G}$ mice compared with wt mice. H&E staining of the indicated organs of the 17-week-old mice was performed as described in the Materials and Methods section. Scale bar, 100 μm (lung, muscle, liver, intestine, and bone) and 50 μm (kidney, heart, and aorta). The *arrow* indicates infiltrated inflammatory cells in each organ and degeneration of aortic myocytes or the femoral growth plate. To see this illustration in color, the reader is referred to the web version of this article at www.liebertpub.com/ars

vascular disease. However, this phenotype was not observed in young (5 and 8 weeks old) $SOD3_{R213G}$ mice (data not shown). In addition, aged $SOD3_{R213G}$ mice showed a thin and irregular degenerative growth plate in the femur (Fig. 7C, second row, second panel), which causes irregular trabecular bone to impair proper bone growth in the hind leg, leading to the observed abnormal gait. Again, this phenotype was not observed in young $SOD3_{R213G}$ mice (data not shown). Similar phenotypes were observed in SOD3 Ko mice, but their levels were comparably mild (data not shown). However, wt, SOD3 Tg, and SOD3 lacking HBD mice did not exhibit these phenotypes (data not shown). Taken together, $SOD3_{R213G}$ mice are sensitized to infection and organ degeneration upon aging due to uncontrolled inflammation (Fig. 8). Therefore, these results suggest that the arginine 213 of SOD3 is essential for the protection of normal tissues from inflammation and organ degeneration.

Discussion

Our study demonstrated that the SOD3 variant, R213G, which naturally occurs in man leading to a heart failure phenotype, alters the function of SOD3 in $SOD3_{R213G}$ Tg mice with the same phenotype, namely degeneration of aortic myocytes. Importantly, earlier studies have shown that SOD3 protects against destructive ROS effects in tissues (22, 23). Thus, arginine 213 in the HBD of SOD3 is critical for its proper functioning to maintain normal cell and tissue protection against ROS. While the Tg mice, expressing SOD3 lacking HBD, have a similar phenotype to SOD3 Tg mice, a functionally different role of SOD3 was observed in $SOD3_{R213G}$ Tg mice. In agreement with this finding, it was reported that SOD3 reduces superoxide levels and improves aortic relaxation in response to acetylcholine after LPS treatment, but the

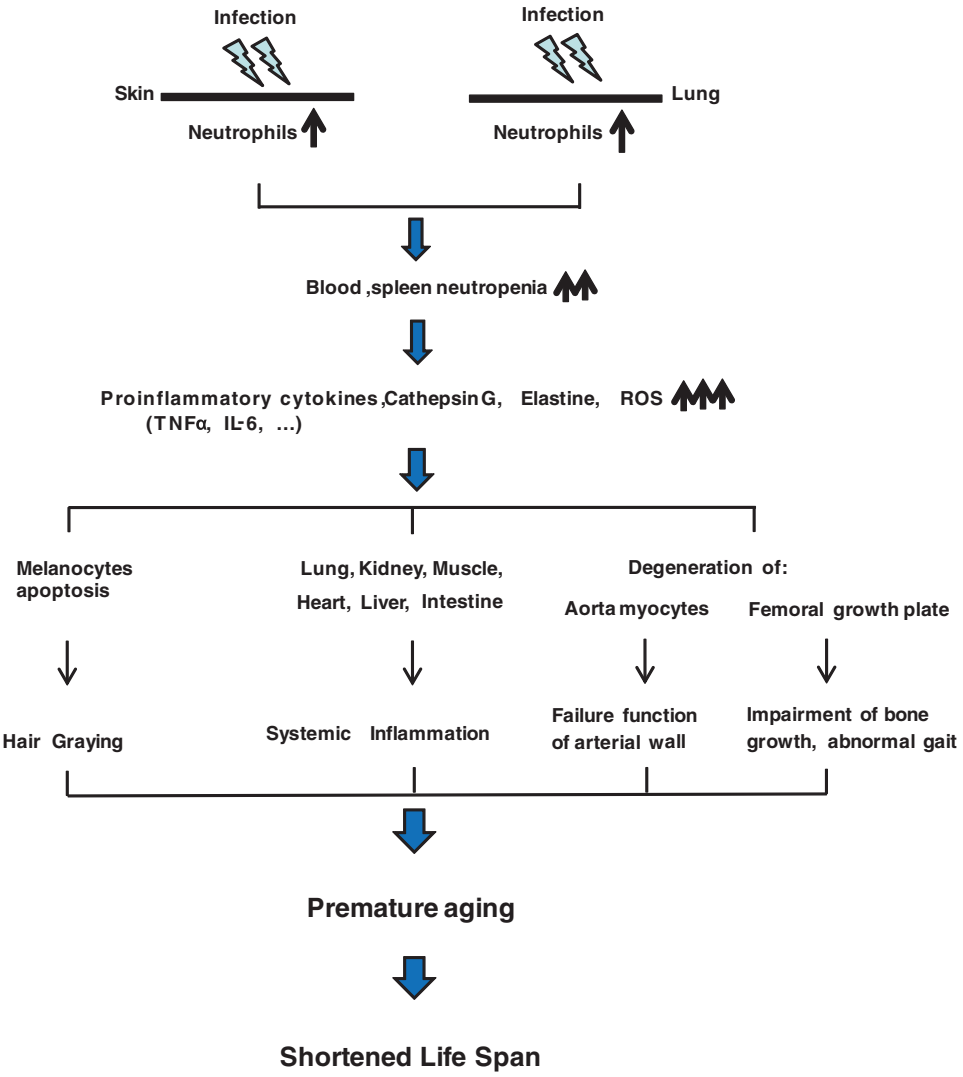

FIG. 8. Proposed model showing that aged $SOD3_{R213G}$ mice exhibit premature aging and are susceptible to neutrophil-mediated inflammation. The skin and lung of aged $SOD3_{R213G}$ mice are susceptible for infection, which leads to recruitment and infiltration of neutrophils into the organs, producing proinflammatory molecules and ROS. Subsequently, these molecules contribute to melanocyte apoptosis leading to hair graying; chronic inflammation leading to systemic inflammation; degeneration of aortic myocytes leading to failure function of the arterial wall; and degeneration of femoral growth plates leading to impairment of bone growth and abnormal gait. Consequently, these lead to shortened life span in mice. To see this illustration in color, the reader is referred to the web version of this article at www.liebertpub.com/ars

$SOD3_{R213G}$ fails to protect against endothelial dysfunction (25). In addition, it was shown that $SOD3_{R213G}$ impairs the affinity of SOD3 to heparin and adherence to the endothelial cell surface, but does not affect the enzymatic activity of SOD3 (1, 39), suggesting that the altered function of the mutant may not simply be due to changes in enzymatic activity, but due to dislocation of SOD3 from the ECM. In agreement, it has been reported that R213G in SOD3 is located in the center of the carboxyl-terminal cluster of positively charged amino acid residues of the HBD and this mutation reduces heparin affinity, tissue SOD3-specific activity (39), and its tissue half-life, resulting in increased plasma levels of SOD3 (8, 15). Consistently, it was reported that R213G disrupts the α-helical structure of SOD3, which leads to reducing the affinity of SOD3 for heparin and collagen and altering its ECM-binding region (34). Therefore, this loss of SOD3 function in $SOD3_{R213G}$ Tg mice may lead to the progressive pathogenesis in organs that require SOD3 for homeostasis.

Since SOD3 controls the levels of extracellular ROS (24), $SOD3_{R213G}$ may fail this function. Thus, as ROS accumulates in the ECM, danger signals are triggered, leading to inflammation, tissue remodeling, and even oncogenesis. These events may lead to many degenerative processes such as apoptosis that worsen with aging. In agreement with this idea, it was reported that while wt cellular fibronectin promotes cell survival, cellular fibronectin mutated in its HBD triggers apoptosis in fibroblasts (20). In this manner, arginine 213 in the HBD of SOD3 is likely to be a crucial site for the proper function of SOD3. Therefore, the inappropriate function of $SOD3_{R213G}$ is, at least in part, due to the loss of its interaction with heparin or heparin sulfate in ECM where SOD3 controls ROS levels. This, consequently, leads to fatal problems at the cells, including aorta and bone, which required SOD3 for protection against tissue ROS. Thus, it is likely that mutant $SOD3_{R213G}$ is a trigger for these inflammatory and degenerative diseases. Perhaps, the role of $SOD3_{R213G}$ on vascular impairments in man (11, 19) may be, in part, due to these consequences. Thus, further investigation is necessary to determine if overcoming the deleterious effects of $SOD3_{R213G}$ may be a therapeutic strategy to treat certain inflammatory and degenerative diseases.

Given that ROS in ECM elicits a danger signal, it is possible that the imbalanced ROS content in $SOD3_{R213G}$-expressing cells may lead to cell death. In agreement, it was reported that

while superoxide plays a signaling role in phagocytes by activating the protease, SOD modulates this signaling event (37). While lower levels of ROS promote cell survival and proliferation, higher levels of ROS activate apoptotic signaling to remove cells that have lost proper cellular function (16). Therefore, imbalances of ROS content in $SOD3_{R213G}$ mice may disrupt proper cellular and tissue functions. Specifically, uncontrolled ROS levels produced by neutrophils in aged $SOD3_{R213G}$ mice may, in part, lead to expression of the phenotype of $SOD3_{R213G}$ mice, including hair graying, systemic inflammation, and cellular degeneration.

Interestingly, the chronic inflammatory phenotype occurred in both aged $SOD3_{R213G}$ mice and SOD3 Ko mice. However, this phenotype was comparably mild in SOD3-deficient mice. Perhaps, this discrepancy is due to the rescue of the SOD3 Ko mice by using alternative molecular mechanisms that maintain proper cellular or organ function. Alternatively, there may be some functional redundancy among the SOD family members, including SOD1 and SOD2 in SOD3 Ko mice. On the other hands, the $SOD3_{R213G}$ mutant mice are greatly overexpressed by the $SOD3_{R213G}$ gene, which may govern endogenous SOD3, altering SOD3 function, affecting its affinity for heparin, or inducing a conformational change of SOD3 in the ECM. In agreement, we observed an increase in the plasma level of SOD3 in the $SOD3_{R213G}$ Tg mice. In addition, it has been reported that mice with an embryonic deletion in SOD3 can tolerate ambient oxygen, whereas those with an acute deletion of SOD3 suffer from severe lung damage and high mortality in ambient oxygen (18). Similarly, $SOD3_{R213G}$ mice may exhibit a more severe phenotype compared with SOD3 Ko mice. On the same line, we observed that SOD3 with deleted HBD mice have a similar phenotype of SOD3 Tg. When we tested *in vitro* for the anti-inflammatory effect using a plasmid encoding SOD3 with deleted HBD or its recombinant protein, the results were similar as those of the full-length SOD3 (data not shown). Thus, we speculated that SOD3 with deleted HBD has a similar function as SOD3 physiologically, allowing the function of endogenous SOD3. Thus, we need to investigate further for this effect.

It is clear that aged $SOD3_{R213G}$ mice display an aging-associated phenotype. In this case, when the tumor suppressor, p53, is deleted in the first six exons of the p53 gene that encodes a carboxy-terminal p53 fragment, this mutation consistently activates p53 and the resultant p53 mutant mice exhibit enhanced resistance to spontaneous tumor development. However, upon aging, the p53 mutant mice display aging-associated phenotypes, reducing longevity, osteoporosis, organ atrophy, and diminished stress tolerance (43). Although young mutant p53 mice did not show this phenotype, significant differences were shown in the skin, hair, and muscle mass in 24-month-old p53 mutant mice. Thus, similar, but not all, aging-associated phenotypes were observed in 17-week-old $SOD3_{R213G}$ mice. This premature aging of $SOD3_{R213G}$ mice may also be controlled by the p53-mediated signaling pathway. Interestingly, a splice variant of $p52^{shc}/p46^{shc}$, the $p66^{shc}$ adaptor protein, enhanced resistance to oxidative stress response and led to an increased life span in mammals (31). In addition, melanocyte-specific deleted *c-Myc* leads to constitutive gray hair in mice (35). Moreover, *Wnt* signaling leads melanocyte stem cells to initiate pigmented hair generation (36) and plays essential roles in the development of melanocytes (12, 13). Thus, SOD3 may also participate in these signal transduction pathways that regulate the proliferative or apoptotic response and life span in mammals. In that sense, it is likely that arginine 213 in the HBD of SOD3 plays a key role in determining the direction of signaling events.

The current study provides a new paradigm for the role of SOD3 in chronic and degenerative diseases, including aging, and may provide a new target to cure systemic inflammation and certain degenerative diseases. In addition, we reported for the first time that SOD3 regulates innate immunity by ameliorating infection and controlling proper signal propagation and activation of neutrophils. Therefore, this animal model will be useful in testing novel therapies to control inflammatory and degenerative diseases.

Materials and Methods

Animals

All mice, including C57BL/6, SOD3 Tg, SOD3 lacking HBD Tg, SOD3 Ko, and $SOD3_{R213G}$ Tg mice, were cared in semispecific pathogen-free conditions, and animal experiments were performed in accordance with established institutional guidance that was approved by the Research Animal Care Committee of The Catholic University (Seoul, Korea). Thus, three to four mice each of wt, SOD3 Tg, SOD3 lacking HBD, SOD3 Ko, and $SOD3_{R213G}$ Tg mice were used for an animal experiment. For the Kaplan–Meier survival curve, each of the forty wt or $SOD3_{R213G}$ mice was monitored.

Transgene insertion

To determine the exact location of insertion of transgenes within the genome, tail DNA of founder #47 and #44 was obtained. The DNAs were digested by restriction endonuclease enzyme digestion and followed sequential PCR to produce amplicons, representing regions flanking the integrated transgene (9). Sequencing and BLAST (Ensemble and NCBI) search were performed to find the locus of integrated genes.

Melanin content in the skin

Dorsal skin of the mice was incubated with 1:3 dispase/trypsin (50 U/ml dispase, Roche, 0.25% Trypsin; GIBCO) for 2 h at 37°C. The skin was chopped and filtered through a 100-μm strainer to remove hair and cornified layers. The separated single cells were subjected to FACS analysis to detect the population of melanocytes using PE-conjugated Melan A antibody (Santa Cruz, CA).

Transient transfection of Melan A cells

Melan A cells were seeded 1 day before transfection. The cells were transiently transfected with a plasmid encoding human SOD3, SOD3 lacking HBD, $SOD3_{R213G}$ mutant, or vector control, using Attractene transfection reagent (GIBCO, Invitrogen, San Diego, CA). To access cell proliferation, 12-h transfected cells were treated with 50 n*M* PMA for 72 h, and the cell number was counted. Apoptotic cells were assessed by staining with Annexin V and propidium iodide (PI). To assess gene expression, 12-h transfected cells were treated with 50 n*M* PMA for 12 h and *Thy*, *MITF*, *Dct*, *c-Myc*, *cyclin D1*, and *Bax* expression was assessed by quantitative RT-PCR (qRT-PCR).

Quantitative RT-PCR

To perform qRT-PCR, the following mouse primers were used. *Tyrosinase*, 5′-gggatagcagatccttctca, 3′-cattggcttctggg taaact; *dopachrome tautomerase*, 5′-gaccctgtgtttgtggtcct, 3′-gttgctctgcggttaggaag; *MITF*, 5′-caagtcccaagcagtggaa, 3′-ggagcttaacggaggcttg; *c-Myc*, 5′-cgactccgtacagccctat, 3′-cgcaacataggatggagag; *cyclin D1*, 5′-cctgacaccaatctcctca, 3′-gacctcctcttcgcacttc; neutrophil secreting elastase, 5′-ctctggct gccatgctact, 3′-gttcacacagtgggctgct; cathepsin G, 5′-cggcagc aactgactaagc, 3′-caagcactcagcccttctg; *TERT*, 5′-gttcctgttctgg ctgatg, 3′-cttgtgacagctcccgtag; and MMP-1, 5′-caccactgaattt caccag, 3′-gaactgcttgtccaggttt. The primers used for TNFα, MCP-1, and MIP1α were described previously (22).

Tissue histology and ultrastructure examination

The tissues, including dorsal skin, lung, kidney, liver, intestine, aorta, muscle, and heart, were isolated and fixed in 4% paraformaldehyde in PBS and embedded in paraffin according to general histochemical procedure. For the skeletal histochemical examination, the femur and tibia were isolated and fixed in 4% paraformaldehyde in PBS overnight, followed by decalcification with 10% formic acid for Hematoxylin and Eosin (H&E) staining. Blood and BALF in the lung were obtained from the mice as described previously (23). Deep quick staining, H&E, or Masson's trichrome staining were followed according to the manufacturer's instructions. Tissue inflammation was assessed based on pathology criteria. Specifically, skin inflammation was assessed by investigating the degree of thickness of the epidermis and the content of infiltrated cells into the skin, fibrosis, and abnormal ECM structure, including collagen accumulation. Immunofluorescence staining of skin was performed with fluorescence-conjugated antibodies against CD11b (BioLegend, San Diego, CA), NIMP-R14 (Abcam, Cambridge, UK), and Melan A (Santa Cruz, CA). Nuclei were stained with DAPI (Vector Lab, Burlingame, CA). The images were taken by confocal microscopy (Carl Zeiss, Thomwood, NY).

To examine the ultrastructure, transmission electron microscopy (TEM) analysis was performed. Skin tissues were fixed in 4% paraformaldehyde and 2.5% glutaraldehyde in 0.1 *M* phosphate buffer for 12 h, and postfixed with 1% osmium tetroxide in PBS for 1 h. TEM analysis was performed as described previously (23). The ultrathin sections (60–70 nm) were obtained by ultramicrotome (Leica Ultracut UCT, Wetzlar, Germany). Ultrathin sections collected on grids (200 mesh) were examined in TEM (JEM 1010, Tokyo, Japan) at 60 kV. The images were recorded by CCD camera (SC 1000; Gatan, Pleasanton, CA).

Cell surface and intracellular staining

APC-conjugated antimouse Ly-6G (Gr1), CD11c, IL-4, IL-17, and IFNγ, PE-conjugated anti-mouse CD11b, IL-17, TNFα, and IL-13, and FITC-conjugated anti-mouse CXCR4, IL-6, and CD4 were purchased from eBioscience (San Diego, CA). PI and FITC-conjugated Annexin V were obtained from BioLegend (San Diego, CA). Cell surface, Gr1, CD11c, CD11b, CXCR4, Annexin V, and PI were measured by flow cytometry (FACS Calibur; BD Bioscience, San Jose, CA). Cytokines, TNFα, IFNγ, IL-4, IL-13, and IL-17, were assessed by flow cytometry after intracellular staining with permeabilizing reagent (BD Cytofix/Cytoperm). The data were analyzed with CellQuest software (Becton Dickinson, Mountain View, CA).

Proliferation of bone marrow neutrophils

$Gr1^+$ $CD11b^+$ neutrophils were isolated from bone marrow (BM) cells and purified using antibody–magnetic bead depletion. In brief, total BM cells from femurs and tibias were flushed out with 2 ml of RPMI 1640 media using a 23-gauge needle. RBC was depleted with hemolysis buffer (Sigma, St Louis, MO) and purified using the lineage cell depletion kit (Miltenyi Biotec, Bergisch Gladbach, Germany). The cells were cultured with 20 ng/ml G-CSF (Prospec, Brunwick, NJ) for 10 days to assess proliferation. The morphology of neutrophils was examined by a light microscope. At some experiments, BM cells were used.

Neutrophil chemotaxis assay

Transwell plates of 3-μm pore size (Corning Costar, Cambridge, MA) were loaded with 600 μl of the medium in the presence of 100 n*M* fMLP in the lower chamber in triplicates. Freshly isolated neutrophils were resuspended at 2×10^7 cells/ml, and 250 μl of this suspension was placed in the inserts in the upper chamber. After 2 h of incubation at 37°C in a 5% CO_2 incubator, migrated cells in the lower chamber were counted by adding 50 μl of 70 m*M* EDTA to release adherent cells.

Immunoblot

Human SOD3 antibody was obtained from Abcam (Cambridge, MA). Blood was lysed and SDS-PAGE was performed using the corresponding antibody for specific protein.

Measurement of ROS content and SOD activity

ROS generation of neutrophils was accessed by staining with H_2DCFH-DA, 2′, 7′-dichlorofluorescein diacetate (5 μ*M*), and FACS analysis was followed. For SOD activity, the fresh blood was taken and subjected to centrifugation for isolation of serum, and SOD activity was measured using the SOD assay kit (Dojindo lab, Kumamoto, Japan).

Statistical analysis

Results are given as the mean ± SD. Data were analyzed by ANOVA at $p < 0.05$ and Scheffe's *post hoc* test or *t*-test ($*p < 0.001$). Differences with a low *p*-value were regarded as statistically significant.

Acknowledgments

The authors thank Professor John Shively (Dept. of Immunology, City of Hope Medical Center, Duarte, CA) for critical reading and editing of the manuscript. This research was supported by the Bio and Medical Technology Development Program of the National Research Foundation (NRF) funded by the Ministry of Science, ICT and Future Planning (NRF-2013-M3A9A3050567) of the Republic of Korea.

Author Disclosure Statement

The authors declare no conflicts of interest exist.

References

1. Adachi T, Yamada H, Yamada Y, Morihara N, Yamazaki N, Murakami T, Futenma A, Kato K, and Hirano K. Substitution of glycine for arginine-213 in extracellular-superoxide dismutase impairs affinity for heparin and endothelial cell surface. *Biochem J* 313 (Pt 1): 235–239, 1996.
2. Arcaroli JJ, Hokanson JE, Abraham E, Geraci M, Murphy JR, Bowler RP, Dinarello CA, Silveira L, Sankoff J, Heyland D, Wischmeyer P, and Crapo JD. Extracellular superoxide dismutase haplotypes are associated with acute lung injury and mortality. *Am J Respir Crit Care Med* 179: 105–112, 2009.
3. Arck PC, Overall R, Spatz K, Liezman C, Handjiski B, Klapp BF, Birch-Machin MA, and Peters EM. Towards a ''free radical theory of graying'': melanocyte apoptosis in the aging human hair follicle is an indicator of oxidative stress induced tissue damage. *Faseb J* 20: 1567–1569, 2006.
4. Belaaouaj A, Kim KS, and Shapiro SD. Degradation of outer membrane protein A in *Escherichia coli* killing by neutrophil elastase. *Science* 289: 1185–1188, 2000.
5. Bennett DC, Cooper PJ, and Hart IR. A line of non-tumorigenic mouse melanocytes, syngeneic with the B16 melanoma and requiring a tumour promoter for growth. *Int J Cancer* 39: 414–418, 1987.
6. Bentley NJ, Eisen T, and Goding CR. Melanocyte-specific expression of the human tyrosinase promoter: activation by the microphthalmia gene product and role of the initiator. *Mol Cell Biol* 14: 7996–8006, 1994.
7. Bowler RP, Arcaroli J, Crapo JD, Ross A, Slot JW, and Abraham E. Extracellular superoxide dismutase attenuates lung injury after hemorrhage. *Am J Respir Crit Care Med* 164: 290–294, 2001.
8. Bowler RP, Nicks M, Olsen DA, Thogersen IB, Valnickova Z, Hojrup P, Franzusoff A, Enghild JJ, and Crapo JD. Furin proteolytically processes the heparin-binding region of extracellular superoxide dismutase. *J Biol Chem* 277: 16505–16511, 2002.
9. Bryda EC and Bauer BA. A restriction enzyme-PCR-based technique to determine transgene insertion sites. *Methods Mol Biol* 597: 287–299, 2010.
10. Butterfield TA, Best TM, and Merrick MA. The dual roles of neutrophils and macrophages in inflammation: a critical balance between tissue damage and repair. *J Athl Train* 41: 457–465, 2006.
11. Chu Y, Alwahdani A, Iida S, Lund DD, Faraci FM, and Heistad DD. Vascular effects of the human extracellular superoxide dismutase R213G variant. *Circulation* 112: 1047–1053, 2005.
12. Dorsky RI, Moon RT, and Raible DW. Control of neural crest cell fate by the Wnt signalling pathway. *Nature* 396: 370–373, 1998.
13. Dunn KJ, Brady M, Ochsenbauer-Jambor C, Snyder S, Incao A, and Pavan WJ. WNT1 and WNT3a promote expansion of melanocytes through distinct modes of action. *Pigment Cell Res* 18: 167–180, 2005.
14. Emerit I, Filipe P, Freitas J, and Vassy J. Protective effect of superoxide dismutase against hair graying in a mouse model. *Photochem Photobiol* 80: 579–582, 2004.
15. Enghild JJ, Thogersen IB, Oury TD, Valnickova Z, Hojrup P, and Crapo JD. The heparin-binding domain of extracellular superoxide dismutase is proteolytically processed intracellularly during biosynthesis. *J Biol Chem* 274: 14818–14822, 1999.
16. Fiers W, Beyaert R, Declercq W, and Vandenabeele P. More than one way to die: apoptosis, necrosis and reactive oxygen damage. *Oncogene* 18: 7719–7730, 1999.
17. Folz RJ and Crapo JD. Extracellular superoxide dismutase (SOD3): tissue-specific expression, genomic characterization, and computer-assisted sequence analysis of the human EC SOD gene. *Genomics* 22: 162–171, 1994.
18. Gongora MC, Lob HE, Landmesser U, Guzik TJ, Martin WD, Ozumi K, Wall SM, Wilson DS, Murthy N, Gravanis M, Fukai T, and Harrison DG. Loss of extracellular superoxide dismutase leads to acute lung damage in the presence of ambient air: a potential mechanism underlying adult respiratory distress syndrome. *Am J Pathol* 173: 915–926, 2008.
19. Juul K, Tybjaerg-Hansen A, Marklund S, Heegaard NH, Steffensen R, Sillesen H, Jensen G, and Nordestgaard BG. Genetically reduced antioxidative protection and increased ischemic heart disease risk: the Copenhagen City Heart Study. *Circulation* 109: 59–65, 2004.
20. Kapila YL, Wang S, and Johnson PW. Mutations in the heparin binding domain of fibronectin in cooperation with the V region induce decreases in pp125(FAK) levels plus proteoglycan-mediated apoptosis *via* caspases. *J Biol Chem* 274: 30906–30913, 1999.
21. Kolaczkowska E and Kubes P. Neutrophil recruitment and function in health and inflammation. *Nat Rev Immunol* 13: 159–175, 2013.
22. Kwon MJ, Han J, Kim BH, Lee YS, and Kim TY. Superoxide dismutase 3 suppresses hyaluronic acid fragments mediated skin inflammation by inhibition of toll-like receptor 4 signaling pathway: superoxide dismutase 3 inhibits reactive oxygen species-induced trafficking of toll-like receptor 4 to lipid rafts. *Antioxid Redox Signal* 16: 297–313, 2012.
23. Kwon MJ, Jeon YJ, Lee KY, and Kim TY. Superoxide dismutase 3 controls adaptive immune responses and contributes to the inhibition of ovalbumin-induced allergic airway inflammation in mice. *Antioxid Redox Signal* 17: 1376–1392, 2012.
24. Kwon MJ, Kim B, Lee YS, and Kim TY. Role of superoxide dismutase 3 in skin inflammation. *J Dermatol Sci* 67: 81–87, 2012.
25. Lund DD, Chu Y, Brooks RM, Faraci FM, and Heistad DD. Effects of a common human gene variant of extracellular superoxide dismutase on endothelial function after endotoxin in mice. *J Physiol* 584: 583–590, 2007.
26. Lund DD, Gunnett CA, Chu Y, Brooks RM, Faraci FM, and Heistad DD. Gene transfer of extracellular superoxide dismutase improves relaxation of aorta after treatment with endotoxin. *Am J Physiol Heart Circ Physiol* 287: H805–H811, 2004.
27. Marklund SL. Extracellular superoxide dismutase and other superoxide dismutase isoenzymes in tissues from nine mammalian species. *Biochem J* 222: 649–655, 1984.
28. Marklund SL. Human copper-containing superoxide dismutase of high molecular weight. *Proc Natl Acad Sci U S A* 79: 7634–7638, 1982.
29. Marklund SL, Holme E, and Hellner L. Superoxide dismutase in extracellular fluids. *Clin Chim Acta* 126: 41–51, 1982.
30. Marklund SL, Nilsson P, Israelsson K, Schampi I, Peltonen M, and Asplund K. Two variants of extracellular-superoxide dismutase: relationship to cardiovascular risk factors in an unselected middle-aged population. *J Intern Med* 242: 5–14, 1997.

31. Migliaccio E, Giorgio M, Mele S, Pelicci G, Reboldi P, Pandolfi PP, Lanfrancone L, and Pelicci PG. The p66shc adaptor protein controls oxidative stress response and life span in mammals. *Nature* 402: 309–313, 1999.
32. Murray PJ and Wynn TA. Protective and pathogenic functions of macrophage subsets. *Nat Rev Immunol* 11: 723–737, 2011.
33. Nathan C. Neutrophils and immunity: challenges and opportunities. *Nat Rev Immunol* 6: 173–182, 2006.
34. Petersen SV, Olsen DA, Kenney JM, Oury TD, Valnickova Z, Thogersen IB, Crapo JD, and Enghild JJ. The high concentration of Arg213—>Gly extracellular superoxide dismutase (EC-SOD) in plasma is caused by a reduction of both heparin and collagen affinities. *Biochem J* 385: 427–432, 2005.
35. Pshenichnaya I, Schouwey K, Armaro M, Larue L, Knoepfler PS, Eisenman RN, Trumpp A, Delmas V, and Beermann F. Constitutive gray hair in mice induced by melanocyte-specific deletion of c-Myc. *Pigment Cell Melanoma Res* 25: 312–325, 2012.
36. Rabbani P, Takeo M, Chou W, Myung P, Bosenberg M, Chin L, Taketo MM, and Ito M. Coordinated activation of Wnt in epithelial and melanocyte stem cells initiates pigmented hair regeneration. *Cell* 145: 941–955, 2011.
37. Reeves EP, Lu H, Jacobs HL, Messina CG, Bolsover S, Gabella G, Potma EO, Warley A, Roes J, and Segal AW. Killing activity of neutrophils is mediated through activation of proteases by K+flux. *Nature* 416: 291–297, 2002.
38. Sandstrom J, Karlsson K, Edlund T, and Marklund SL. Heparin-affinity patterns and composition of extracellular superoxide dismutase in human plasma and tissues. *Biochem J* 294 (Pt 3): 853–857, 1993.
39. Sandstrom J, Nilsson P, Karlsson K, and Marklund SL. 10-fold increase in human plasma extracellular superoxide dismutase content caused by a mutation in heparin-binding domain. *J Biol Chem* 269: 19163–19166, 1994.
40. Schiffmann E, Corcoran BA, and Wahl SM. N-formylmethionyl peptides as chemoattractants for leucocytes. *Proc Natl Acad Sci U S A* 72: 1059–1062, 1975.
41. Stralin P, Karlsson K, Johansson BO, and Marklund SL. The interstitium of the human arterial wall contains very large amounts of extracellular superoxide dismutase. *Arterioscler Thromb Vasc Biol* 15: 2032–2036, 1995.
42. Tobin DJ and Paus R. Graying: gerontobiology of the hair follicle pigmentary unit. *Exp Gerontol* 36: 29–54, 2001.
43. Tyner SD, Venkatachalam S, Choi J, Jones S, Ghebranious N, Igelmann H, Lu X, Soron G, Cooper B, Brayton C, Park SH, Thompson T, Karsenty G, Bradley A, and Donehower LA. p53 mutant mice that display early ageing-associated phenotypes. *Nature* 415: 45–53, 2002.
44. Yao H, Arunachalam G, Hwang JW, Chung S, Sundar IK, Kinnula VL, Crapo JD, and Rahman I. Extracellular superoxide dismutase protects against pulmonary emphysema by attenuating oxidative fragmentation of ECM. *Proc Natl Acad Sci U S A* 107: 15571–15576, 2010.
45. Yasumoto K, Yokoyama K, Takahashi K, Tomita Y, and Shibahara S. Functional analysis of microphthalmia-associated transcription factor in pigment cell-specific transcription of the human tyrosinase family genes. *J Biol Chem* 272: 503–509, 1997.

Address correspondence to:
Prof. Tae-Yoon Kim
Department of Dermatology
The Catholic Research Institute
of Medical Science, Rm. 4003
Seoul 137-701
Republic of Korea

E-mail: tykimder@catholic.ac.kr
mjkwon7@hanmail.net

Date of first submission to ARS Central, July 12, 2014; date of final revised submission, March 24, 2015; date of acceptance, April 15, 2015.

Abbreviations Used

BALF = bronchoalveolar lavage fluid
Dct = dopachrome tautomerase
ECM = extracellular matrix
fMLP = formyl-methionyl-leucyl-phenylalanine
HBD = heparin-binding domain
LDL = low-density lipoprotein
MCP-1 = monocyte chemotactic protein 1
MITF = microphthalmia transcription factor
MMP-1 = matrix metalloproteinase-1
ROS = reactive oxygen species
SOD3 = extracellular superoxide dismutase
TERT = telomerase reverse transcriptase
Tyr = tyrosinase